ELSEVIER

Chemical Engineering Journal 130 (2007) 135–145

Chemical Engineering Journal

www.elsevier.com/locate/cej

Comparison of ML–EM algorithm and ART for reconstruction of gas hold-up profile in a bubble column

Ashutosh K. Patel, Ashwin W. Patwardhan, Bhaskar N. Thorat *

Chemical Engineering Department, Institute of Chemical Technology (ICT), N. M. Parekh Road, Matunga (E), Mumbai, Maharashtra 400019, India

Abstract

Algebraic reconstruction technique (ART) and maximum likelihood–expectation maximization (ML–EM) algorithm have been applied for image reconstruction using gamma-ray tomography. This methodology can be of immense help in establishing the hydrodynamics of several multiphase systems such as two-phase and three-phase bubble column reactors. The effect of various image processing parameters such as initial guess, grid size, stopping criteria and gamma-ray measurement parameters like beam configuration, number of projection, number of views on the quality of reconstructed image has been studied in present work. It has been observed that ML–EM algorithm shows more precise and faster results as compared to ART and it serve as a preferential tool in image reconstruction. These techniques were then used in the estimation of gas hold-up profile in a two-phase aqueous system. Average gas hold-up values in bubble column based on reconstructed local hold-up values based on the above two techniques were found to be in good agreement with the experimental data within ±10% accuracy, however, ML–EM algorithm may be preferred due to better capability of incorporating the modalities of data collection.

Keywords: Gamma-ray scanning; Gas hold-up; Multiphase system; Attenuation

1. Introduction

Facile construction, absence of moving part, low operating cost and easy operation makes bubble columns a highly attractive gas–liquid contactor. Detailed understanding of hydrodynamics of bubble column is needed for the design and development of an optimized and trouble free operation of the reactor. In bubble column, gas hold-up is an important hydrodynamic parameter as the knowledge of radial as well as axial gas hold-up distribution gives rise to pressure variation resulting in a characteristic liquid circulation in a bubble column. This intern governs the rate of mixing, heat and mass transfer. Gas hold-up information also facilitates the determination of the flow regimes such as homogeneous, transition and heterogeneous regimes.

Computed tomography (CT) is one such technique that is capable of providing the hold-up distribution of the phases in a multiphase system by exploring the object from many different directions. The impact of this technique in process tomography has been considered to be revolutionary in troubleshooting, design and development of multiphase system. Neal and Bankhoff [1] were the first to measure the radial hold-up profiles in a two-phase flow using electro resistivity probe. Thereafter, several measurement techniques have been reported using conductivity probe, electro-resistivity probe, optical probe, hot-film anemometer, particle image velocimetry (PIV), ultrasonic techniques, electrical capacitance, resistance tomography and gamma-ray attenuation techniques. Joshi et al. [2] have reviewed these techniques extensively in their recent publication.

Fundamentally, hold-up distribution reconstruction is a mathematical problem dealing with measured line integrals at different angles and directions in a suitable mathematical form and solving it [3]. The image reconstruction algorithms may be analytical or iterative in nature [3–5]. Analytical algorithms are known to be fast and generally based on transform techniques such as Fourier transform, Filter back projection method, Abel transform and so on. Their disadvantage is the need of large number of noiseless data uniformly distributed over 180° or 360° to produce results with a desired accuracy [6]. Also, their lies difficulty to model the physics and statistical characteristics of the data acquisition process [7]. Whereas, the iterative algorithm has good flexibility for various beam configurations. It can precisely incorporate the model of physics and statistics of gamma-ray tomography and the literature shows that it works well with noisy data and a limited number of path integrals,

* Corresponding author. Tel.: +91 22 24145616x289; fax: +91 22 24145614.
E-mail address: bnt@udct.org (B.N. Thorat).

1385-8947/$ – see front matter © 2006 Elsevier B.V. All rights reserved.
doi:10.1016/j.cej.2006.06.015

Nomenclature

a	element of system matrix/weighted matrix
A	attenuation
d	distance of projection from the center of column
D_d	detector aperture
H_D	dispersed liquid height
H_L	clear liquid height
I	intensities of the emerging beam
I_o	intensities of the incident beam
l_{ij}	the length of jth projection in the ith pixel
M	total number of projections
n	constant
N	total number of pixels
p	projection
$\bar{p}$	projection estimated
r	radial location
R	radius of column
S	system matrix
t	thickness of absorbing medium
X_d	distance of scattering event from the detector
z_j	the number of pixels through which jth projection passes

Greek letters

ε_G	gas hold-up
$\bar{\varepsilon}_G$	column/cross-sectional average gas hold-up
ε_{GW}	gas hold-up at wall
θ	source angle
μ	attenuation coefficient

Subscripts

a	air
chodl	chordal gas hold-up
i	number of pixel
j	number of projection
k	number of iteration
l	liquid
reco	reconstructed value
w	water/wall
TP	two phase

albeit slow [8]. Dempster et al. [9] have reported the use of EM algorithm for solving incomplete data problems, but it was not until Shepp and Vardi [10], that the EM algorithm was applied to emission and transmission tomography. Using these techniques extensive research was carried out in the field of emission tomography to get faster and better image quality [11–15]. Transmission tomography such as GRT was initially used mostly for non-distractive applications where it is possible to obtain the complete data set and analytical methods can give faster and better results in such applications. Algebraic techniques were also applied successively for similar applications [16,17].

The present literature is bereft of the technicalities involved in the use of ART and ML algorithm, particularly for the application of phase distribution in multiphase systems. Also several image reconstruction parameters such as; initial guess, grid size, and beam configuration have not been studied in detail for ML algorithm. In present study, the comparison of ART and ML algorithm has been carried out using several measurement parameters such as beam configuration, number of views and number of projection. The influence of other parameters such as initial guess and grid size was also studied with the help of reconstructed distribution of the linear water attenuation coefficient values and gas hold-up profile.

2. Gamma-ray tomography: underlying principle

Gamma-ray emitted during the radioactive decay process penetrate through the multiphase system area and these can be detected by the scintillation detectors placed on the opposite side of the source. Detector catches the coincidentally emitted γ-rays and the location of the attenuation taken place inside the volume between the source and the detector. The attenuation is a function of the attenuation coefficient, μ, (which in turn depends on the energy possessed by gamma photons) and the thickness of the absorber. It can be expressed as follow:

$$A = -\ln\left(\frac{I}{I_o}\right) = \int \mu \, dt \tag{1}$$

where I_o and I are the intensities of the incident and emerging beams, respectively, μ the linear attenuation coefficient, t the thickness of the absorbing medium and A is the attenuation. From Eq. (1), it can be seen that the attenuation A and the attenuation coefficient μ are linearly related. The attenuation of the projection through a bubble column filled with gas, liquid and gas–liquid medium can be given by the following expressions:

$$\ln\left(\frac{I_a}{I_o}\right) = -(\mu_a t_a + \mu_w 2t_w) \tag{2}$$

$$\ln\left(\frac{I_l}{I_o}\right) = -(\mu_l t_l + \mu_w 2t_w) \tag{3}$$

$$\ln\left(\frac{I_{TP}}{I_o}\right) = -(\mu_a t_a + \mu_l t_l + \mu_w 2t_w) \tag{4}$$

where I_a, I_l and I_{TP} are the intensities of the emerging beam from air, liquid and two-phase system, respectively; μ_a and μ_l are the linear attenuation coefficients of air and liquid, respectively, and t_a, t_l and t_w are the thickness of air, liquid and wall medium, respectively.

Chordal gas hold-up of each measured projection, which is a linear integration of the local hold-up over projection path can be obtained using the following expression based on the above three equations,

$$\varepsilon_{chodl} = \frac{\ln(I_{TP}/I_l)}{\ln(I_a/I_l)} \tag{5}$$

The spatial distribution of gas hold-up can be reconstructed using a suitable reconstruction algorithm provided the spatial variation of the chordal gas hold-up across the interested system area at several radial and angular locations is known.

3. Image reconstruction

Iterative methods used for the estimation of attenuation distribution, can be expressed using the following equation:

$$P_j = \sum_{i=1}^{N} a_{i,j}\mu_i \tag{6}$$

where p_j is the total attenuation measured at jth projection, N the total number of pixels and μ_i is the attenuation coefficient value of ith pixel. $a_{i,j}$ is elements of system matrix or weighted matrix given by, $S = [a_{i,j}] \in \Re^{M\times N}$, which enables the iterative reconstruction method to recover resolution that was lost in the projections due to measurement uncertainties. Fundamentally, iterative algorithm finds the solution of Eq. (6) by successive iterations. Iterations progresses based on the comparison of current estimate with the measured projections. The iterative algorithms like ART and ML–EM algorithm differs in the way the measured and estimated projections are compared and the kind of corrections applied to the current estimate. The procedure is repeated until the estimated attenuation distribution is consistent with the measured projections. In short, using iterative algorithm, the difference between the measured path integral hold-up and the calculated hold-up from reconstructed pixel values is minimized.

3.1. Geometric considerations

As source and detectors were collimated, each projection is represented by a line, which is at source angle θ and d distance away from the center of column and expressed as $p(d, \theta)$, as shown in Fig. 1. The attenuation measured at various angular and radial locations over the cross-section represented by a vector, **P**, is given as $[p_j; j = 1, \ldots, M]$, where M is the number of projections. The quantity $\mu(x, y)$ is defined as the estimated attenuation at any point (x, y) of the transverse slice. This unknown quantity, $\mu(x, y)$, is assumed to be proportional to the distribution of the phases in the area of interest. The projection, $p(d, \theta)$ is the sum of the attenuations of gamma-ray energy recorded in a given time interval along the straight line between the detector and source.

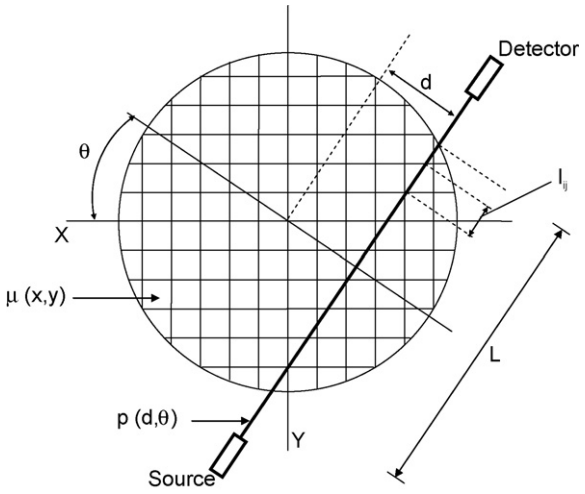

Fig. 1. Schematic diagram for estimation of system matrix.

Several methods have been studied by number of researcher for the calculation of system matrix [18,19]. In the present work, system matrix was calculated based on the geometrical position of pixels in which the entire object was divided and the projections taken at different locations (Fig. 1). The element of system matrix, a_{ij} can be expressed as:

$$a_{ij} = \frac{l_{ij}}{\sum_{j=1}^{M} l_{ij}} \tag{7}$$

where l_{ij} is the length of jth projection in the ith pixel. A specific grid size and a beam configuration represented by an identical system matrix is then estimated only once in order to save computational time.

3.2. Selection of initial guess

In the implementation of the iterative algorithm based on image reconstruction, the process was initiated by arbitrarily creating a first estimate of the spatial distribution of the attenuation coefficient known as initial guess. The initial guess can be a uniform image initialized to 0 or 1 (depending on whether the correction is carried out under the form of an addition or multiplication) or a distribution enclosed in the field of view. In ML algorithm, first guess should be a positive non-zero number because a negative value does not make any sense and also because each new value is found by multiplying the current values. It should be noted that any value set initially to zero will remain zero throughout. In the present study, the initial guess distribution was obtained using three different concepts:

1. An averaged back projection estimation of the unknown local attenuation coefficient μ_i, in ith pixel can be written as:

$$\mu_i = \frac{1}{M}\sum_{j=1}^{M} p_{ij} \tag{8}$$

where p_{ij} is the value of the jth projection passing through the ith pixel.

2. The minimum projection method (MPM) is a simple non-linear modification of Eq. (8) and it can be expressed as:

$$\mu_i = \min(p_{i1}, p_{i2}, \ldots, p_{iM}) \tag{9}$$

3. Modified back projection method preserves the total number of counts and it is similar to the back projection estimation method and it can be expressed as:

$$\mu_i = \frac{1}{M}\sum_{j=1}^{M} \frac{p_{ij}}{z_j} a_{ij} \tag{10}$$

where z_j is the number of pixels through which jth projection passes and a_{ij} is the system matrix element.

3.3. Maximum likelihood–estimation maximization (ML–EM) algorithm

The ML algorithm finds the best estimate for the solution by fitting a criterion of maximization of the likelihood of reconstructed image. This was done by dividing each iteration of the algorithm in two steps: in the expectation step (E step), the formula expressing the likelihood of any reconstructed image for a given measured data is formed, and in the maximization step (M step), the image that has the greatest likelihood to give the measured data was found [20]. The log likelihood over all projections can be represented as:

$$\ln f_{\mathrm{ML}}(\mathbf{P}, \mu) = \sum_j \left\{ -c_j \, \mathrm{e}^{-\sum_i a_{ij}\mu_i} - p_j \sum_i a_{ij}\mu_i + p_j \ln c_j - \ln p_j! \right\} \tag{11}$$

where c_j is the total number of gamma-ray photons leaving the source. The derivation of expectation and maximization step of the log-likelihood function has been described by Lange and Carson [21]. Accordingly, at every iteration, a current estimate is used for the estimation of projections. The measured projections were then compared with the estimated projections, and the ratio between these two was used to modify the current estimate to produce a more accurate updated figure, which intern becomes the next iteration.

3.4. Algebraic reconstruction technique (ART)

The ART algorithm is simply based on corrective technique. Each projected density is thrown back across the reconstruction space in which the densities are iteratively modified to bring each reconstructed projection into agreement with the measured projection. The estimated projection is subtracted from the measured projection and used further to estimate the accurate attenuation distribution by incorporating difference between the two in the current estimate. Mathematically, the algorithm can be defined by the following equation [16,17]:

$$\mu_i^{k+1} = \mu_i^k + \frac{p_j - \bar{p}_j}{\sum_{i=1}^N a_{ij}} a_{ij} \tag{12}$$

3.5. Optimizing number of iterations

In the proposed iterative reconstruction method of ML–EM algorithm and ART, the converging rate was found to be higher until certain point and thereafter the converging rate becomes slower. An iterative method needs very large number of iterations to completely match the reconstructed image with the actual image. In the case of excessively higher number of iterations, the statistical noise gets added to the reconstructed image and the quality of distribution deteriorates. Therefore, for a successful implementation of the iterative algorithm, it becomes pertinent to use certain termination criteria to identify the optimal image quality and stop the iterations so that the image deterioration is avoided.

RMS (root mean square) error was estimated from the actual and reconstructed pixel values, given by Eq. (13). For simulated data, pixel values were used for RMS estimation known as pixel RMS. For actual experimental data, projection values were used for RMS known as overall RMS, which can be expressed as:

$$\mathrm{RMS} = \sqrt{\frac{\sum_{i=1}^N (\mathrm{Actual} - \mathrm{Reconstructed})^2}{\sum_{i=1}^N (\mathrm{Reconstructed})^2}} \tag{13}$$

A lower value of RMS indicates a better agreement between the reconstruction and actual values. Zero value of RMS is an ideal and a perfect agreement between the measured and reconstructed data. Therefore, RMS, below a certain threshold value, can be used logically as stopping criteria. In iterative methods, the updating term progresses to unity (in ML algorithm) and to zero (in ART) and the function gets optimized, which can also be used as a pixel level stopping criterion. Such a study for ML algorithm for emission tomography has been reported in detail by Kontaxakis and Tzanakos [22] but never applied for the multiphase systems.

4. Experimental procedure

In the present study, a bubble column of 0.2 m diameter having specification given in Fig. 2 was used. Fan and parallel beam configuration data were generated by calculating as well as by scanning the two-phase and the single-phase system. These data were then used for the estimation of gas hold-up and linear water attenuation coefficient distribution to study the behavior of ART and ML algorithm.

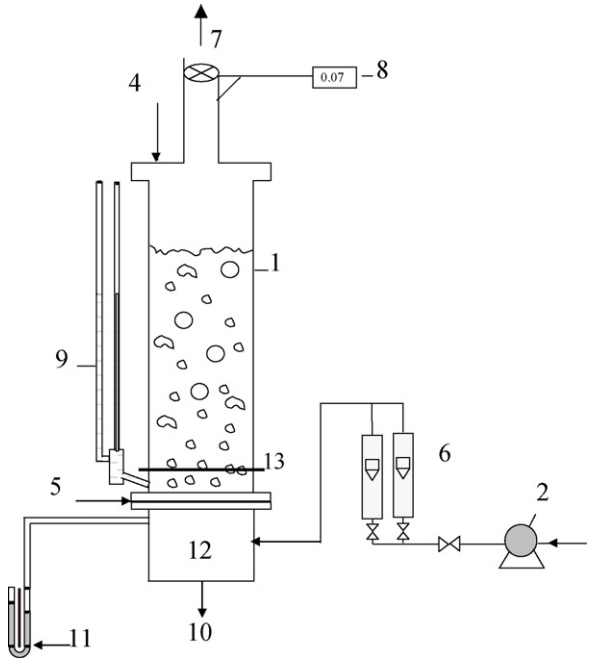

Fig. 2. Experimental setup. (1) Bubble column; (2) air compressor; (3) air inlet; (4) liquid inlet; (5) pipe sparger; (6) rotameter; (7) turbine anemometer; (8) anemometer display; (9) clear liquid tube; (10) liquid drain; (11) U-tube manometer; (12) gas chamber; (13) gamma-ray scanning location, H/D = 0.3.

4.1. Linear water attenuation coefficient

A bubble column of 0.2 m diameter was used to obtain the water attenuation coefficient under the condition of column being filled with only water. Projection data was generated in a parallel as well as fan beam configuration. For this purpose, the projection vector was estimated at each source-detector position. The projections for reconstruction of distribution of the linear water attenuation coefficient can be then given by the equation proposed by Swift et al. [23], which accounts for scattering effects, expressed as:

$$\frac{I}{I_o} = e^{-\mu t} + 0.5\left(\frac{D_d}{X_d}\right)^2 (1 - e^{-\mu t}) \quad (14)$$

where D_d and X_d are the detector aperture and the distance of scattering event from the detector, respectively.

4.2. Gas hold-up profile

In this case, an axisymmetric gas hold-up distribution was calculated in a 0.2 m bubble column using Eq. (15) for radial variation of fractional gas hold-up, originally proposed by Uyema and Miyauchi [24]:

$$\varepsilon_G = (\bar{\varepsilon}_G - \varepsilon_{GW})\left(\frac{n+2}{n}\right)\left[1 - \left(\frac{r}{R}\right)^n\right] + \varepsilon_{GW} \quad (15)$$

where r is the radial location, R the radius of column and $\bar{\varepsilon}_G$ is the column average gas hold-up. $\bar{\varepsilon}_G$ was taken as 0.289 (experimentally observed by bed expansion) at superficial gas velocity 0.19 m/s, ε_{GW} is the gas hold-up at wall taken as 0.05 and the value of n as 2.6 [25]. Using Eqs. (14) and (15), the calculated projection values were used for the reconstruction of the gas hold-up profile.

4.3. Gamma-ray tomography experiments

Scanned data was generated by actual gamma-ray scanning of the Perspex cylindrical bubble column of 0.2 m i.d. and 1.2 m height as shown in Fig. 2. Perforated plate was used as a sparger having 1% free area and 1 mm hole diameter. Superficial gas velocity was varied in the range of 0–0.19 m/s. Column was filled with 0.6 m clear liquid height. Gamma-ray scanning system (Fig. 3) consists of 1 mCi ^{137}Cs gamma source (disc source of 0.02 m diameter), sodium iodide (NaI) with thallium (Tl) activated scintillation detectors (BICRON), photo multiplier tube, a pre-amplifier, a multi-channel (eight channels) analyzer, data acquisition system and related hardware and software. Source collimator having a slit, 0.03 m long and 0.003 m in thickness was used. Circular collimators, 0.087 m in diameter, were used for detectors and the collimator slit was 0.035 m long and 0.004 m in thickness. Numbers of trial runs were conducted with different combinations of dwell time and number of events. A dwell time of roughly 15 s was necessary to satisfactorily capture the steady state dynamic behavior of flow patterns prevailing in a bubble column, especially at higher superficial gas velocity. The two-phase counts were checked with the background counts. Based on these preliminary results, the number of events and dwell time were fixed at 50 and 15 s, respectively. This gave reproducibility of measurements within ±2%. The total acquisition time for each source location measurement was 750 s. Restriction on the requirement of a minimum dwell time would necessitate a reduction in the number of events, reducing the total scan time.

Fan beam configuration was used for reconstruction of the gas hold-up profile. Compton scattering, a phenomenon which contributes noise in the GRT measurements became the incoming gamma-ray photons deflects through an angle with respect to its original direction. Therefore, gamma-ray photon energy partially or completely gets transferred to electron energy and results in a sudden and abrupt change in gamma-ray photons existence. The distance between the source and the detector is less in fan beam scanning (near wall region) and there is a possibility to detect the low energy scattered photons by detectors. For a fan beam scanning, standard counted photons due to scattering was 5% of the total counted photons and this can even go high (up to 50%) as the distance between source and detector decreases, resulting in more error [4]. For this reason, in the

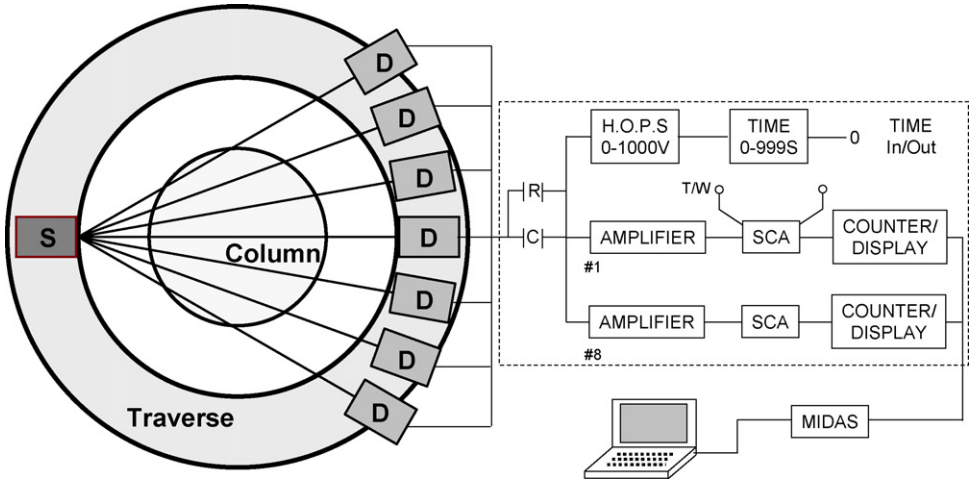

Fig. 3. Gamma-ray scanning system: (S) 1 mCi ^{137}Cs gamma source and (D) 1 in. NaI(Tl) detector.

present GRT measurements source was kept 0.12 m away from the center of the column and detectors were placed on an arc of radius 0.44 m, as shown in Fig. 3. The average fractional gas hold-up in bubble column was estimated from the global bed expansion technique as follows:

$$\bar{\varepsilon}_G = \frac{H_D - H_L}{H_D} \quad (16)$$

Gas hold-up and water attenuation distribution were reconstructed using ART and ML algorithm from the scanned data on 11×11 and 22×22 grids. In case of parallel beam configuration (PBC), calculations were carried out at 3, 6 and 9 angular views equiangularly placed over 360° and each view having nine projections (equally spaced at 0.02 m) and 19 projections (equally spaced at 0.01 m). In case of fan beam configuration (FBC), calculations and measurements were done at 3, 5, 6 and 9 angular views equiangularly placed over 360° and each view having nine projections (equiangular at 6°) and 17 projections (equiangular at 3°). Fig. 4A and B shows the source and detector location for one angular view in parallel and fan beam configuration, respectively.

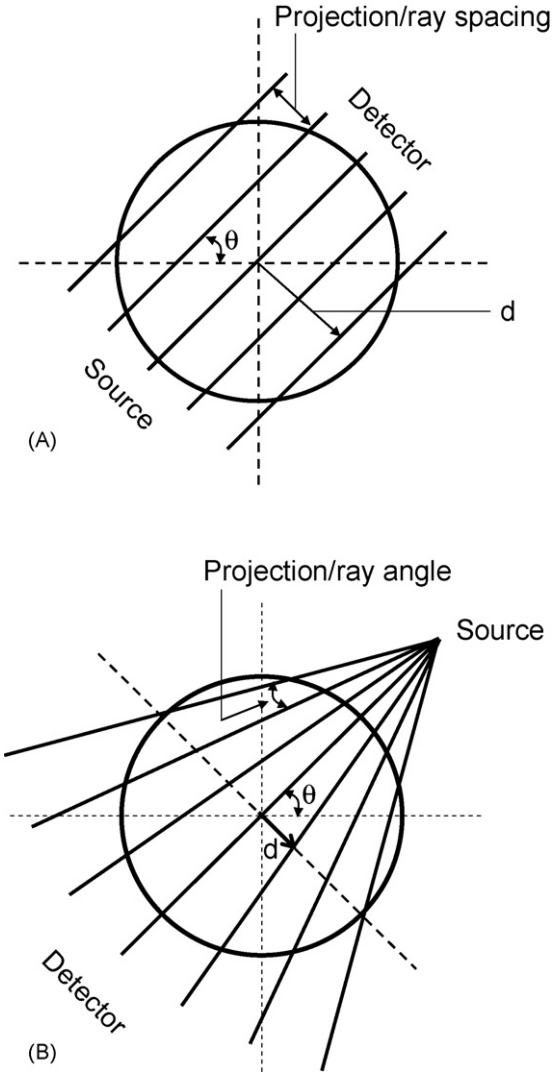

Fig. 4. Beam configuration for gamma-ray scanning: (A) parallel beam configuration and (B) fan beam configuration.

5. Results and discussions

Projection data obtained in Section 4.1 was used to estimate the distribution of the linear water attenuation coefficient. Influence of initial guess on quality of reconstructed distribution of the linear water attenuation coefficient values has been studied. The results show that initial guess value does not affect the computation time, whereas the quality of distribution of the reconstructed linear water attenuation coefficient values changes significantly. Fig. 5A and B shows the distribution of the reconstructed linear water attenuation coefficient by ML algorithm and ART, respectively. It can be seen from Fig. 5A that about 72%, 81% and 82% pixels have μ_w value within ±5% error for initial guess using average back projection (ABP), minimum projection method (MPM) and modified back projection (MBP), respectively. On the other hand, completely reverse trend was observed for ART as about 80%, 77% and 76% pixels having μ_w value within ±5% error for initial guess using ABP, MPM and MBP, respectively. The standard deviation values as shown in Table 1 supports the above observations. Based on these finding, it was desired to use the modified back projection method in ML algorithm and the average back projection method in ART. It gives better results as compared to the other two methods as can be seen from Table 1. Here, the value of standard deviation

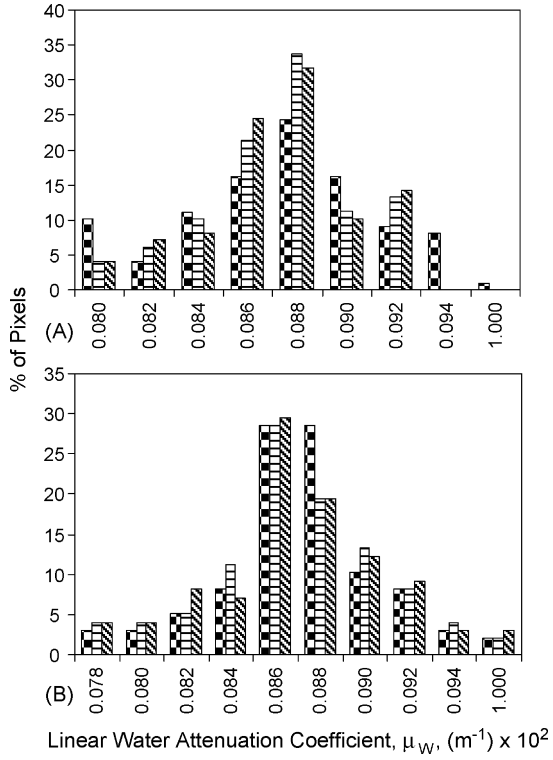

Fig. 5. Distribution of linear water attenuation coefficient in reconstructed image using fan beam configuration (17 projections and three views)—initial guess as parameter. (▞) ABP, average back projection; (▤) MPM, minimum projection method; (▚) MBP, modified back projection. (A) ML–EM algorithm and (B) ART.

Table 1
Effect of initial guess value (17 projections and three views in fan beam configuration)

Initial guess method	ML–EM algorithm		ART	
	Mean	S.D.	Mean	S.D.
Average back projection	0.0857	0.0055	0.086	0.0044
Minimum projection	0.0861	0.0045	0.086	0.0051
Modified back projection	0.0861	0.0042	0.086	0.0052

is 0.0042 for MBP in case of ML–EM algorithm and 0.0044 for the case of ABP in ART method. Likhachov et al. [17] have reported similar observations by using ART method.

Beam configuration and grid size were found to affect the quality of the distribution of the reconstructed linear water attenuation coefficient values because various combinations of these two causes a significant variation in the system matrix properties. Distribution of the linear water attenuation coefficient values was reconstructed using both parallel and fan beam configuration data to visualize the effect of beam configuration. Distribution of the linear water attenuation coefficient value in reconstructed image is as shown in Fig. 6A and B for ML algorithm and ART, respectively. It can be seen that all pixels of reconstructed image by ML algorithm and ART have μ_w values within ±5% deviation for parallel beam configuration data. Whereas only 82% and 77% pixels have ≤±5% deviation in reconstructed image using

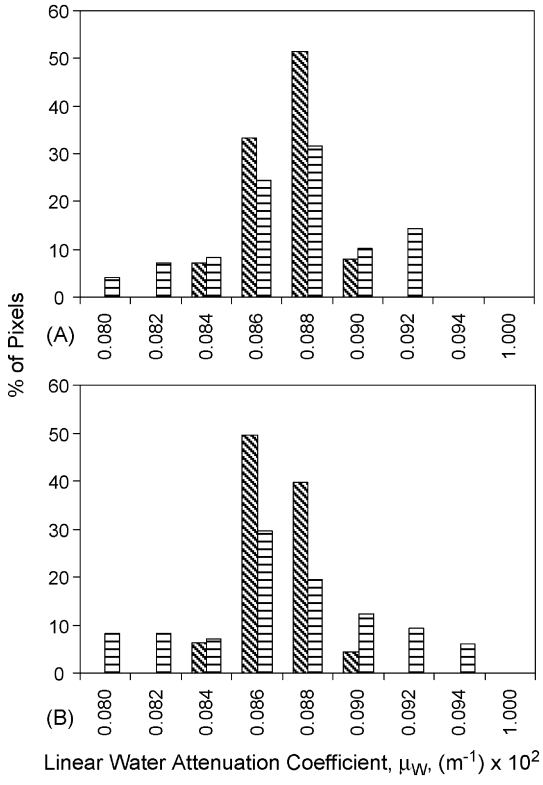

Fig. 6. Distribution of linear water attenuation coefficient in reconstructed image—beam configuration as parameter. (▨) PBC, parallel beam configuration and (▤) FBP, fan beam configuration. [Nineteen projections and three views in PBC and 17 projections and three views in FBC.] (A) ML–EM algorithm and (B) ART.

Table 2
Effect of beam configuration (19 projections and three views in parallel beam configuration and 17 projections and three views in fan beam configuration)

Beam configuration	ML–EM algorithm		ART	
	Mean	S.D.	Mean	S.D.
Fan beam configuration	0.0861	0.0042	0.086	0.0052
Parallel beam configuration	0.0859	0.0015	0.0859	0.0017

FBC data by ML algorithm and ART, respectively. Also, lower standard deviation value of reconstructed distribution of the linear water attenuation coefficient using PBC data was observed for both the reconstruction methods as shown in Table 2. In the case where source is placed close to the column, beam overlapping and region of missing data are two commonly encountered situations in fan beam configuration gamma-ray scanning, which is not the case in PBC measurements. This situation leads to the non-uniformity in system matrix and the addition of statistical noise in the measured data in case of FBC data. This might be the probable reason for inaccuracies and distortions of image quality for FBC. Results show that precise and good quality of reconstructed image can be obtained for parallel beam data as compared to the fan beam data. In spite of this, the fan beam configurations have been used extensively in the past because of the less time consumed as compared to the parallel beam measurements for same quality.

As the grid size affects the reconstructed image quality, it becomes necessary to select a suitable grid size for a given projection spacing and configuration. To study the effect of grid size on quality of reconstructed image, the water attenuation coefficient distribution was reconstructed as discussed in Section 4.1. PBC data (19 projections and three views) was used for reconstruction on 11 × 11 grid (having grid size larger than the ray spacing) and 22 × 22 grid (having grid size equal to the ray spacing), whereas 19 projections and nine views PBC data was used for reconstruction on 44 × 44 grid (having grid size smaller than the ray spacing). The reconstructed distribution of μ_w by ML algorithm and ART is as shown in Fig. 7A and B, respectively. All the pixels of reconstructed image on 11 × 11 and 22 × 22 grid have μ_w value within ±5% deviation, whereas, only 11–12% pixels has such accuracy in reconstructed distribution of the linear water attenuation coefficient values on 44 × 44 grid even though more number of views were taken for reconstruction. Table 3 shows the effect of grid size in terms of standard deviation of reconstructed distribution of the linear water attenuation coefficient. Standard deviation value and distribution of the linear water attenuation coefficient

Table 3
Effect of grid size (19 projections in parallel beam configuration and three views for 11 × 11 and 22 × 22 grid size, whereas nine views for 44 × 44)

Grid size	ML–EM algorithm		ART	
	Mean	S.D.	Mean	S.D.
11 × 11	0.0859	0.0015	0.0859	0.0017
22 × 22	0.0860	0.0013	0.0860	0.0015
44 × 44	0.0535	0.0978	0.0529	0.0980

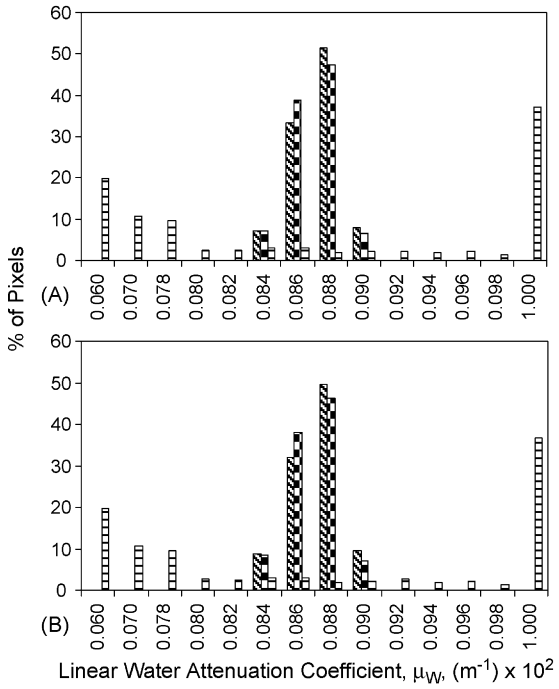

Fig. 7. Distribution of linear water attenuation coefficient in reconstructed image—grid size as parameter. (▨) 11 × 11, (▪) 22 × 22, (▭) 44 × 44 [19 projections in parallel beam configuration and three views for 11 × 11 and 22 × 22 grid, whereas nine views for 44 × 44 grid]. (A) ML–EM algorithm and (B) ART.

values shows that the reconstructed image quality is superior in case of grid size equal to the ray spacing as compared to other two options. In case of grid size smaller than projection spacing, the non-uniform distribution and missing of information of certain elements of system matrix leads to poor quality of reconstructed image. Similar observations were found for the case of gas hold-up reconstruction on 11 × 11 and 22 × 22 grid using FBC data generated by actual scanning of bubble column.

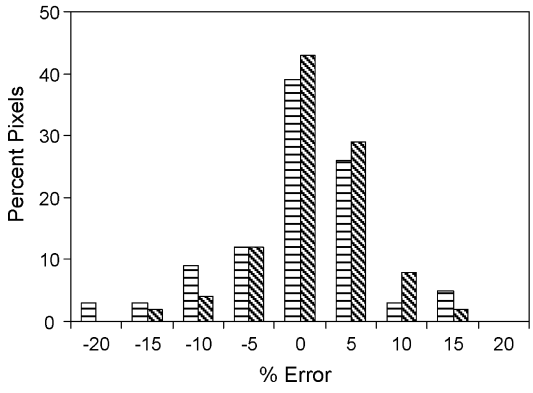

Fig. 8. Distribution of percentage error in pixels of reconstructed gas hold-up. (▭) 11 × 11 and (▨) 22 × 22 (nine projections and five views in fan beam configuration).

Fig. 8 shows the distribution of percentage error in each of the pixels of reconstructed image of gas hold-up distribution. About 84% and 77% pixels have ≤±5% error in reconstructed image of gas hold-up distribution on 22 × 22 and 11 × 11 grid, respectively.

Local gas hold-up was reconstructed using FBC data generated with the help of Eq. (15) to study the effect of number of projections and number of views. Results show good agreement between the measured and reconstructed average gas hold-up values for all combinations of projections and view numbers, as shown in Table 4. Results also show the influence of total number of projections (either by increasing the no of projection per view or no of views itself) on the gas hold-up distribution. From Fig. 9, it can be seen that all sets of projections and views yields good quality of reconstructed images and the agreement between the measured and the reconstructed one-dimensional gas hold-up profile was found to be good. This observation contradicts the distribution of % error estimated based on the reconstructed

Table 4
Estimated gas hold-up using different number of projections and views and error with respect to column average gas hold-up measured by bed expansion technique

Pixels	Projections	Views	ML–EM algorithm		ART	
			$\bar{\varepsilon}_{G,reco}$	Error (%)	$\bar{\varepsilon}_{G,reco}$	Error (%)
9 × 9	5	3	0.274	5.12	0.275	4.84
		5	0.309 (0.192)	6.78 (1.25)	0.305	5.50
		6	0.306	5.81	0.303	4.78
		9	0.305	5.50	0.304	5.09
11 × 11	7	3	0.277	4.05	0.278	3.98
		5	0.282 (0.20)	2.60 (5.41)	0.282	2.39
		6	0.282	2.53	0.282	2.35
		9	0.292	1.07	0.292	1.04
11 × 11	9	3	0.282	2.39	0.281	2.87
		5	0.282 (0.192)	2.39 (1.25)	0.282	2.42
		6	0.293	1.42	–	–
		9	0.284	1.63	0.285	1.49
11 × 11	17	3	0.283	2.08	0.283	2.18
		6	0.293	1.25	0.292	1.14
		9	0.285	1.45	0.282	2.28

Note: Scanned data reconstructed values shown in parenthesis and measured average gas hold-up for scanned data is 0.189.

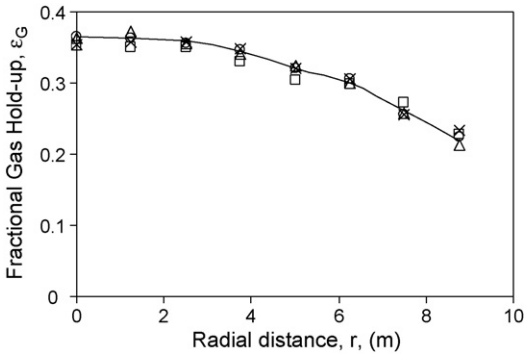

Fig. 9. Fractional gas hold-up (ε_G) vs. radial distance (r). (—) Actual; (□) 9p × 3v; (△) 9p × 5v; (×) 9p × 6v; (◯) 9p × 9v.

2D gas hold-up distribution as shown in Fig. 10A and B. Similar behavior was observed for all other combination of number of projection and views. Results emphasis that it is desired to obtain minimum five views for a given number of projections to reconstruct the gas hold-up distribution with acceptable quality and precision. In reconstructed gas hold-up distribution image, more than 90% pixels having reconstructed values with $\leq\pm10\%$ error for more than five views are as shown in Fig. 10A and B. Fig. 10A and B also shows that further increasing the no of views (from 5 to 9 views), it leads to a better quality of gas hold-up distribution (number of pixels with $\leq\pm10\%$ error increases from 91% to 94%) and it approaches actual distribution. Fig. 11A and B shows the percent error distribution for reconstructed image using various numbers of projections with five views. Similar results were observed for other number of views too. Image reconstruction quality was found to be improved with an increase in the number of projection (number of pixels with $\leq\pm10\%$ error increases from 82% to 93% with an increase in number of projection from 5 to 17). Results also show the level of desired quality and such a precision can be obtained for scanned data (given as bracketed quantity in Table 4).

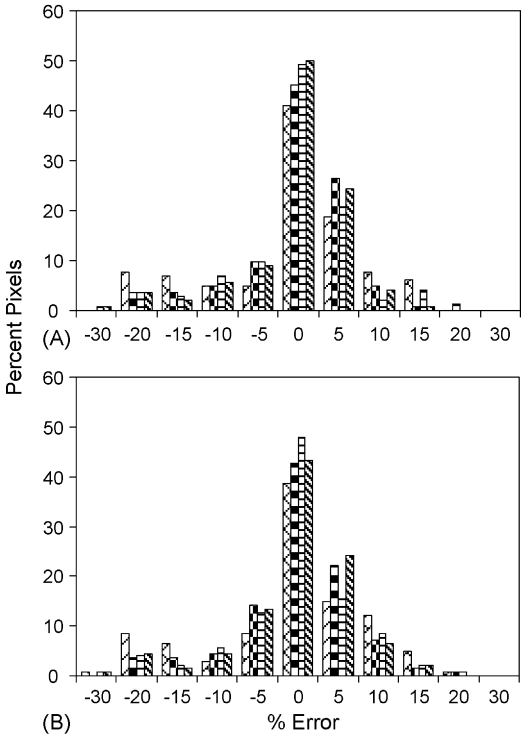

Fig. 10. Distribution of percentage error in pixels of reconstructed gas hold-up—number of views as parameter. (▨) 3 view, (▙) 5 view, (▤) 6 view and (▩) 9 view (nine projections in fan beam configuration). (A) ML–EM algorithm and (B) ART.

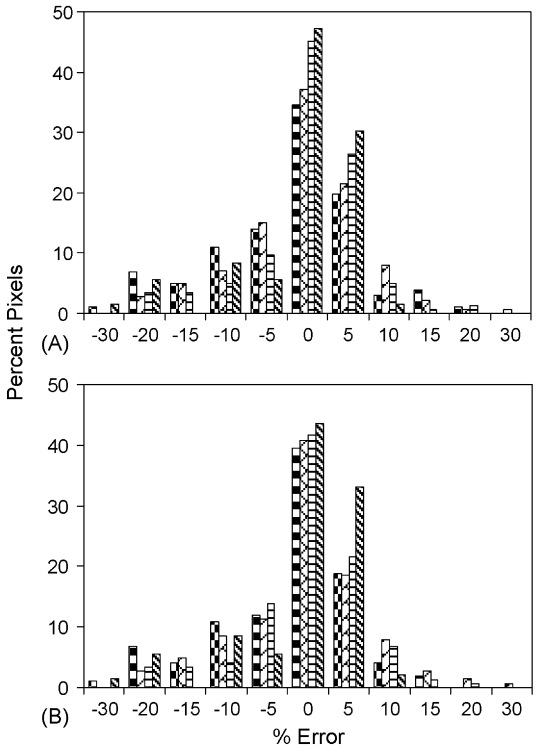

Fig. 11. Distribution of percentage error in pixels of reconstructed gas hold-up—number of projection as parameter. (▙) 5 projection, (▨) 7 projection, (▤) 9 projection and (▩) 17 projection (five views in fan beam configuration). (A) ML–EM algorithm and (B) ART.

The overall stopping criteria was used to terminate the contribution of projection value to the pixels, once the overall RMS value for a specific projection reaches the desired threshold value. Fig. 12A and B shows the plot of RMS verses number of iterations for ML algorithm and ART, respectively. The RMS value approaches near zero at number of iterations $\geq$40 and $\geq$500 for ML algorithm and ART, respectively, indicating the optimum reconstruction image quality (RMS threshold value considered here is 0.003). Initially due to high rate of convergence, RMS quickly reaches to a certain value, which is less than one and it takes more number of iteration to reach the RMS close to the minimum (RMS approach zero). Iteration gets terminated when the RMS value reaches the desired threshold limit. Under these circumstances, the pixel updating factor approaches unity and zero for the case ML–EM algorithm and ART, respectively. Fig. 13A and B shows the graph of percent pixel converged versus number of iterations. This graph gives a better picture of the exact number of iterations for a desired convergence of pixels. For example, to achieve 96% pixels to be converged with the desired threshold limit, ML–EM algorithm

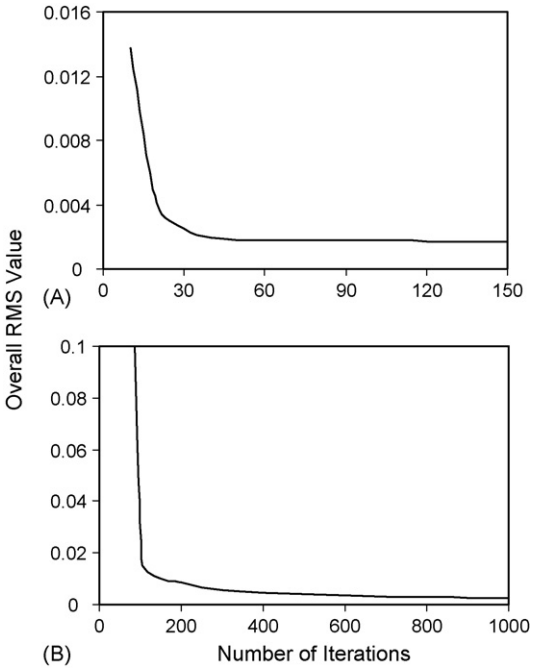

Fig. 12. Overall RMS values vs. number of iterations: (A) ML–EM algorithm and (B) ART.

requires approximately 110 iteration, whereas this number is more than 700 in case of ART. Based on these above findings, it is recommended to use this pixel level stopping criteria for both the methods, however, ML algorithm requires lesser number of iteration and it gives a better quality.

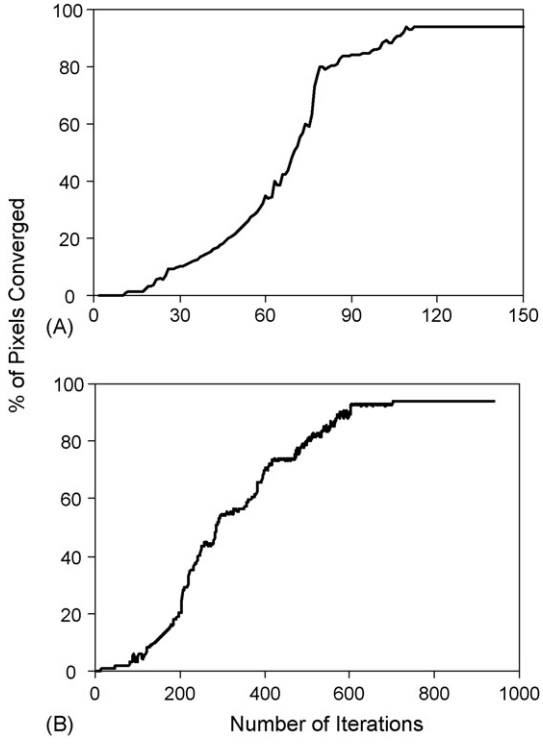

Fig. 13. Percent of pixels converged vs. number of iterations: (A) ML–EM algorithm and (B) ART.

6. Conclusions

- Both ART and ML–EM algorithm provide the reconstruction of gas hold-up and the water attenuation coefficient using parallel beam as well as fan beam configuration data. However, ART needs very large number of iterations as compared to ML–EM algorithm. For the same quality of the reconstructed image, ART requires more than 8–9 times iterations as compared to ML–EM algorithm.
- Although, ML reconstruction is faster, it may deteriorate if proper iteration stopping criteria is not used.
- Initial guess has moderate effect on reconstructed image quality. The average back projection method was found to be better for ART, whereas the modified back projection method exemplifies ML–EM algorithm.
- It is recommended to select the grid size equal to or greater than the projection spacing for obtaining a better quality of reconstructed image.
- The effect of grid size becomes less significant as the number of projections increases. Also, it is necessary to have minimum five views for better reconstructed gas hold-up distribution profile.
- It is highly recommended to use pixel-based stopping criteria instead of overall RMS value to get the desired quality of reconstructed image.

Acknowledgement

Ashutosh Patel would like to acknowledge the support from Department of Atomic Energy-Knowledge Based Engineering.

References

[1] L.G. Neal, S.G. Bankhoff, A high resolution resistivity probe for determination of local void properties in gas–liquid flow, AIChE J. 9 (4) (1963) 490–494.
[2] J.B. Joshi, U.P. Veera, Ch.V. Prasad, D.V.P. Kumar, N.S. Deshpande, S.S. Thakre, B.N. Thorat, Gas hold-up structure in bubble column reactors, Proc. Indian Natl. Sci. Acad. (PINSA) 64 (4) (1998) 441–567.
[3] C. Kak, M. Slaney, Principles of Computerised Tomographic Imaging, IEEE Press, New York, 1988.
[4] G.T. Herman, Image Reconstruction from Projections: The Fundamentals of Computerized Tomography, Academic Press, New York, 1980.
[5] P.P. Bruyant, Analytic, Iterative reconstruction algorithms in SPECT, J. Nucl. Med. 43 (2002) 1343–1358.
[6] P.P. Bruyant, J. San, J.J. Mallet, Streak artifact reduction in filtered back projections using a level line-based interpolations method, J. Nucl. Med. 41 (2000) 1913–1919.
[7] R.M. Lewitt, Reconstruction algorithms: transform methods, Proc. IEEE 71 (1983) 390–408.
[8] Y. Censor, Finite series-expansion reconstruction methods, Proc. IEEE 71 (1983) 409–419.
[9] P. Dempster, N.M. Laird, D.B. Rubin, Maximum likelihood from incomplete data via the EM algorithm, J. Roy. Stat. Soc. 39 (B) (1977) 1–38.
[10] L.A. Shepp, Y. Vardi, Maximum likelihood reconstruction for emission tomography, IEEE Trans. Med. Imag. 2 (1982) 113–119.
[11] L.A. Shepp, Y. Vardi, J.B. Ra, S.K. Hilal, Z.H. Cho, Maximum likelihood PET with real data, IEEE Trans. Nucl. Sci. 31 (2) (1984) 910–913.
[12] R.M. Lewitt, G. Muehllehner, Accelerated iterative reconstruction for positron emission tomography based on the EM algorithm for maximum likelihood estimation, IEEE Trans. Med. Imag. 5 (1) (1986) 16–22.

[13] G. Kontaxakis, G. Tzanakos, Study of certain characteristics of the EM algorithm for image reconstruction in positron emission tomography, in: Proceedings of the 18th Conference on IEEE Northeast Bioengineering, Kingston, RI, 1992, pp. 89–90.
[14] J. Nuyts, P. Suetens, L. Mortelmans, Acceleration of maximum likelihood reconstruction, using frequency amplification and attenuation compensation, IEEE Trans. Med. Imag. 12 (4) (1993) 643–652.
[15] P.E. Kinahan, J.A. Fessler, J.S. Karp, Statistical image reconstruction in PET with compensation for missing data, IEEE Trans. Nucl. Sci. 44 (4) (1997) 1552–1557.
[16] J.M. de Oliveira Jr., Project, construction and test of a mini computerized tomography, Braz. J. Phys. 33 (2) (2003) 273–275.
[17] V. Likhachov, V.V. Pickalov, N.V. Chugunova, V.A. Baranov, Development of iterative algorithms for industrial tomography, in: Proceedings of the 1st World Congress on Industrial Process Tomography, Buxton, Greater Manchester, 1999, pp. 463–469.
[18] R. Maad, G.A. Johansen, Automatic weight matrix generation for gamma-ray tomography, in: Proceedings of the 3rd World Congress on Industrial Process Tomography, Bannf, Canada, 2003, pp. 86–89.
[19] E. Veklerov, J. Llacer, E.J. Hoffman, MLE reconstruction of a brain phantom using a Monte-Carlo probability matrix and a statistical stopping rule, IEEE Trans. Nucl. Sci. 35 (1) (1988) 603–607.
[20] L. Kaufman, Implementing and accelerating the EM algorithm for positron emission tomography, IEEE Trans. Med. Imag. MI-6 (1987) 37–51.
[21] K. Lange, R. Carson, EM reconstruction algorithms for emission and transmission tomography, J. Comput. Assist. Tomogr. 8 (1984) 306–316.
[22] G. Kontaxakis, G. Tzanakos, Study of certain characteristics of the EM algorithm for image reconstruction in positron emission tomography, in: Proceedings of the 18th Conference on IEEE Northeast Bioengineering, Kingston, RI, 1992, pp. 89–90.
[23] W.L. Swift, F.X. Dolan, P.W. Runstadler, Measurements in polyphase flows, in: Processings of the Winter Annual Meeting of ASME, San Fracisco, 1978, p. 25.
[24] K. Uyema, T. Miyauchi, Properties of recirculating turbulent two-phase flow in gas bubble columns, AIChE J. 25 (1979) 258–266.
[25] U.P. Veera, Design of multiphase reactors. Ph.D. Thesis, University of Mumbai, India, 1999.